Available online at www.sciencedirect.com
ScienceDirect
Phytochemistry 68 (2007) 2273–2289
PHYTOCHEMISTRY
www.elsevier.com/locate/phytochem

$^{13}CO_2$ as a universal metabolic tracer in isotopologue perturbation experiments

Werner Römisch-Margl [a], Nicholas Schramek [a], Tanja Radykewicz [a], Christian Ettenhuber [a], Eva Eylert [a], Claudia Huber [a], Lilla Römisch-Margl [a], Christine Schwarz [a], Maria Dobner [c], Norbert Demmel [c], Bernhard Winzenhörlein [c], Adelbert Bacher [a,b], Wolfgang Eisenreich [a,b,*]

[a] *Lehrstuhl für Organische Chemie und Biochemie, Technische Universität München, Lichtenbergstr. 4, D-85747 Garching, Germany*
[b] *Ikosatec GmbH, D-85748 Garching, Germany*
[c] *Amt für Grünordnung und Naturschutz der Stadt Augsburg, Botanischer Garten, Dr.-Ziegenspeck-Weg 10, D-86161 Augsburg, Germany*

Received 4 January 2007; received in revised form 20 March 2007
Available online 15 May 2007

Abstract

A tobacco plant was illuminated for 5 h in an atmosphere containing $^{13}CO_2$ and then maintained for 10 days under standard greenhouse conditions. Nicotine, glucose, and amino acids from proteins were isolated chromatographically. Isotopologue abundances of isolated metabolites were determined quantitatively by NMR spectroscopy and mass spectrometry. The observed non-stochastic isotopologue patterns indicate (i) formation of multiply labeled photosynthetic carbohydrates during the $^{13}CO_2$ pulse phase followed by (ii) partial catabolism of the primary photosynthetic products, and (iii) recombination of the ^{13}C-labeled fragments with unlabeled intermediary metabolites during the chase period. The detected and simulated isotopologue profiles of glucose and amino acids reflect carbon partitioning that is dominated by the Calvin cycle and glycolysis/glucogenesis. Retrobiosynthetic analysis of the nicotine pattern is in line with its known formation from nicotinic acid and putrescine via aspartate, glyceraldehyde phosphate and α-ketoglutarate as basic building blocks. The study demonstrates that pulse/chase labeling with $^{13}CO_2$ as precursor is a powerful tool for the analysis of quantitative aspects of plant metabolism in completely unperturbed whole plants.

1. Introduction

Isotope incorporation studies have an impressive history of success in the analysis of metabolic processes, as well as of some remarkable glitches such as the misassignments of numerous plant and microbial isoprenoids to the mevalonate pathway which are in reality derived from the recently discovered non-mevalonate pathway (for reviews, see Rohmer, 2003; Eisenreich et al., 2004a).

Typical isotope incorporation strategies for metabolic studies generate a non-random state of isotope distribution by the introduction of a single isotopically labeled compound into the experimental system. However, we have shown earlier that it is by no means essential that a single, well-defined isotope-labeled compound should be used for that purpose. For example, highly transparent biosynthetic information can be obtained with a crude mixture of ^{13}C-labeled lipids in the form of a chloroform extract from universally ^{13}C-labeled biomass (Eisenreich et al., 1997).

In a rigorous extension of the concept that the starting conditions for the perturbation/relaxation analysis of metabolic processes can implicate complex mixtures of ^{13}C-labeled compounds as long as the postulate of non-random overall isotope distribution is fulfilled, pulse-labeling of plants on the basis of endogenous photosynthesis from $^{13}CO_2$ may appear as a somewhat unusual approach. However, the use of $^{13}CO_2$ as a precursor in intact plants and

* Corresponding author. Address: Lehrstuhl für Organische Chemie und Biochemie, Technische Universität München, Lichtenbergstr. 4, D-85747 Garching, Germany. Tel.: +49 89 289 13336; fax: +49 89 289 13363.
E-mail address: wolfgang.eisenreich@ch.tum.de (W. Eisenreich).

0031-9422/$ - see front matter © 2007 Elsevier Ltd. All rights reserved.
doi:10.1016/j.phytochem.2007.03.034

the subsequent analysis of multiply ^{13}C-labeled products by NMR were introduced more than 25 years ago by Schaefer and his co-workers (Schaefer et al., 1975, 1980). More specifically, soybean or corn plants were exposed to $^{13}CO_2$. After a chase period, the relative concentrations of $^{12}C^{13}C$ and $^{13}C^{13}C$ pairs in the C-1/C-2 moiety of sucrose or certain carbon pairs in fatty acids were determined from the ^{13}C NMR signals. On the basis of these data, it was concluded that glucose cycling and/or photorespiration were involved in sucrose metabolism and fatty acid biosynthesis. Due to the limited quality of the NMR technology at that time, a comprehensive analysis of the entire labeling pattern was not possible, but it was already stated that "hopefully, more complicated, as yet unsolved, problems in carbon metabolism can also be approached" (Schaefer et al., 1975).

In a subsequent study, Hutchinson and co-workers analysed the biosynthesis of nicotine in *Nicotiana tabacum* plants that were exposed to an atmosphere containing $^{13}CO_2$ for 12–14 h (Hutchinson et al., 1976). After a chase period of 2–10 days, nicotine was isolated and analysed by ^{13}C NMR spectroscopy. Satellite signals due to $^{13}C^{13}C$ coupling indicated the biosynthetic pathway of nicotinic acid *via* a C_3 and a C_2 building block, although the satellite signals could not be unequivocally assigned to distinct isotopologues of nicotine due to the limited resolution of the NMR spectrum at 22.6 MHz. NMR peak areas measured by cutting and weighing of the expanded NMR spectrum suggested an unsymmetrical C_4 precursor for the pyrrolidine ring.

Advances in analytic instrumentation, notably in sensitivity and resolution of NMR and mass spectrometry, now enable a technically advanced concept which is not limited to a specific isotope enrichment in a given metabolic product, but is based on the quantitative assessment of multiple isotopologues (Eisenreich et al., 1991, 1993; Bacher et al., 1999; Szyperski, 1995; Sauer, 2005). However, despite the progress in theory and practice of biosynthetic studies, the $^{13}CO_2$ method was not further exploited for a holistic analysis of metabolic flux in plants to the best of our knowledge.

In this study, we generated ^{13}C-labeled photosynthesis products from $^{13}CO_2$ in a growing tobacco plant and analysed the isotopologue patterns of leaf glucose and of amino acids that were obtained from protein hydrolysates, as well as of nicotine in the wake of the $^{13}CO_2$ pulse. The study shows that the $^{13}CO_2$ technique, in conjunction with advanced analytical techniques for isotopologue quantification and interpretation, opens a gateway for the exploration of a wide variety of metabolic investigations in plants under physiological conditions.

2. Results

2.1. Experimental setting

In our feasibility study, a growing tobacco plant was exposed to an atmosphere of synthetic air containing 600 ppm of $^{13}CO_2$ with white light illumination for 5 h (cf. Fig. 1). The concentration of $^{12}CO_2$ was around 80 ppm during the incubation period. During this period the plant consumed about 1 l of $^{13}CO_2$. From the given $^{13}CO_2/^{12}CO_2$ ratio, a C_6 compound (e.g. hexose phosphate) that is formed from CO_2 during the pulse period should predominantly comprise the $^{13}C_6$-isotopologue (about 47%) as well as six $^{13}C_5$-isotopologues (in total about 38%) (cf. Fig. 2). During the subsequent chase period, the

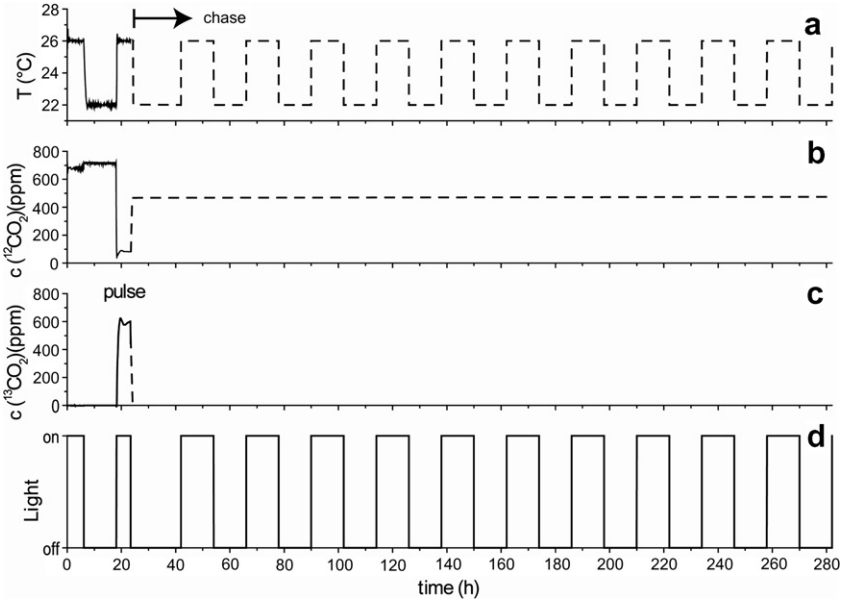

Fig. 1. System parameters of the $^{13}CO_2$ labeling experiment with *N. tabacum*. (a) incubation chamber temperature (°C); (b) concentration of $^{12}CO_2$ (ppm); (c) concentration of $^{13}CO_2$ (ppm); (d) light/dark periods.

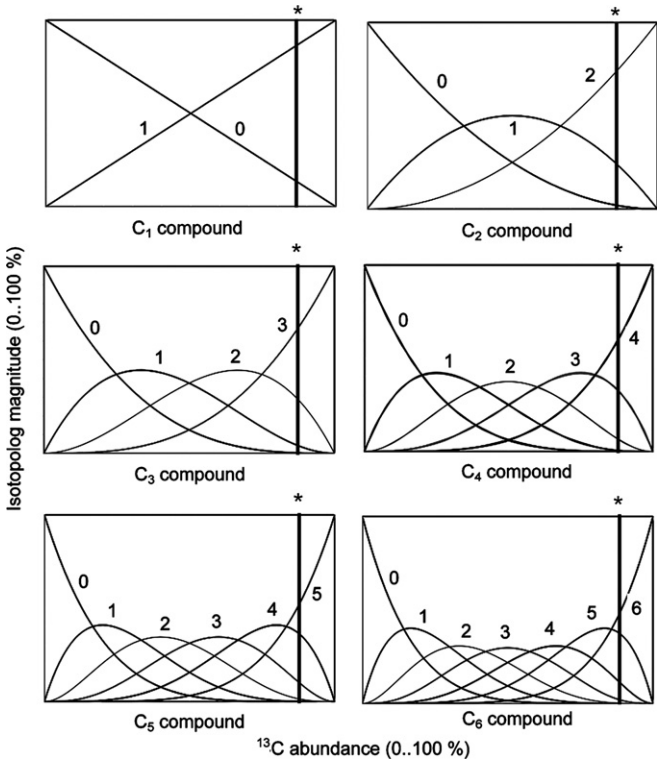

Fig. 2. Stochastic ^{13}C isotopologue distribution in compounds comprising one to six carbon atoms. Numbers indicate the sum of ^{13}C atoms in a given molecule. The abscissa defines the molar ratio of $^{12}C/^{13}C$. The ordinate defines the relative fraction of an isotopologue set. Hypothetical random isotopologue compositions in metabolites biosynthesised exclusively during the pulse phase of the labeling experiment in this study (i.e., by CO_2 fixation in an atmosphere containing $^{12}CO_2$ and $^{13}CO_2$ at a molar ratio of 1:7.5) are indicated by asterisks.

plant was kept in the greenhouse under ambient conditions for 10 days. Nicotine and glucose were then isolated from the leaves, and biosynthetic amino acids were obtained from acid-hydrolyzed leaves by chromatography procedures.

2.2. Isotopologue profile of leaf glucose

The isotopologue composition of glucose was analysed by high-resolution ^{13}C NMR spectroscopy as described earlier (Eisenreich et al., 2004b). In order to describe the complex isotopologue space of glucose, we use a notation where the carbon skeleton of glucose is represented by a six-digit binary number with the first digit representing C-1, the second digit representing C-2, etc.; 1 signifies ^{13}C, 0 signifies ^{12}C, and X or Y signifies either ^{12}C or ^{13}C. For example, $\{11XXXX\}_{glc}$ designates a set of isotopologues carrying ^{13}C in positions 1 and 2, and ^{13}C or ^{12}C in any of the positions 3–6; isotopologue sets of this type are subsequently designated as X-groups. While the labeling status of X positions is totally undefined, the overall number of ^{13}C-labeled atoms in all Y-positions, given outside the brackets of the X-group, might be a known parameter. This expansion of the X-group formalism is not only useful for MS data, as described later, but also in those cases of NMR data that can only be assigned to the sum of two simple X-groups (e.g. $\{011XXX, 110XXX\} = \{Y1YXXX\}^1$).

Earlier, we showed that the abundances of individual isotopologues can be determined from X-group abundances by numerical deconvolution (Eisenreich et al., 2004b; Ettenhuber et al., 2005). Typically, the abundances of 15–25 independent X-groups of glucose can be determined from the NMR signals of α- and β-glucose. In our earlier experiments using [U-$^{13}C_6$]glucose as tracer, it was justified to consider only a set of 21 isotopologues out of the possible 63 ^{13}C-isotopologues of glucose because 42 isotopologues can be assumed to be rarely generated in an experimental setup with unlabeled glucose in high excess over the ^{13}C labeled tracer (for a detailed discussion, see also Eisenreich et al., 2004b; Glawischnig et al., 2002). In those experiments, the number of observed linearly independent X-groups exceeded the number of unknown isotopologue concentrations. Using this approach, it was shown that [U-$^{13}C_6$]glucose is converted in tobacco leaves into a variety of ^{13}C-labeled isotopologues indicating extensive cycling of glucose by the network of primary carbohydrate metabolism (i.e., glycolysis, glucogenesis and the pentose phosphate pathway) (Ettenhuber et al., 2005).

In the present experiment using $^{13}CO_2$ as tracer, this rigorous deconvolution could not be performed due to the fact that, in principle, the formation of all possible 63 ^{13}C-isotopologues of glucose appears possible. On the basis of the detected X-group abundances by NMR spectroscopy (Table 1), the system is clearly underdetermined and additional methods need to be developed in order to assess the required number of 63 independent X-group abundances.

However, even without a detailed evaluation, it is striking that the relative abundances of certain X-groups from the present experiment show considerable similarity with

Table 1
Molar abundances of isotopologue sets (X-groups) in leaf glucose from *Nicotiana tabacum* in the experiment with $^{13}CO_2$

X-group	Molar abundance (mol%)		
	α-glucose	β-glucose	Average
{10XXXX}	1.14	1.14	**1.14**
{11XXXX}	0.46	0.46	**0.46**
{110XX0}	nd	**0.10**	
{111XX1}	nd	**0.17**	
{11YXXY}[1]	nd	**0.19**	
{010XXX}	1.10	1.12	**1.11**
{Y1YXXX}[1]	0.25	0.24	**0.25**
{110XXX}	nd	**0.10**	
{011XXX}	nd	**0.14**	
{111XXX}	0.24	0.25	**0.25**
{X010XX}	**1.10**	nd	
{XY1YXX}[1]	**0.23**	nd	
{X111XX}	**0.28**	nd	
{XXXX01}	1.09	1.08	**1.09**
{XXXX11}	0.52	0.52	**0.52**

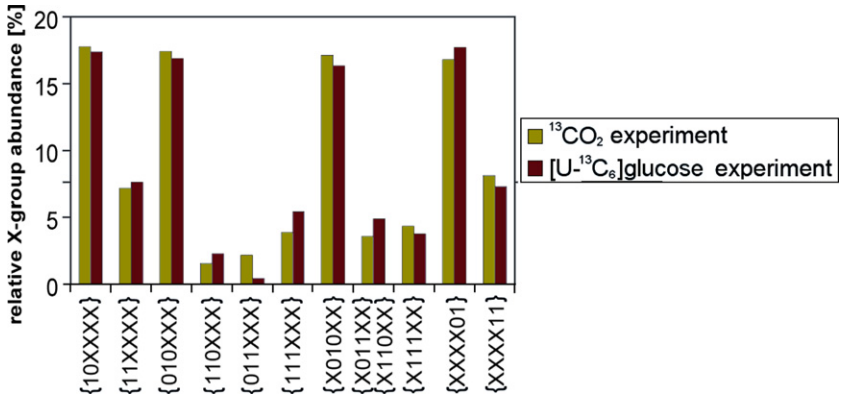

Fig. 3. Comparison of the relative abundances of certain X-groups in leave glucose from the experiment with [U-$^{13}C_6$]glucose (Ettenhuber et al., 2005) and $^{13}CO_2$ from *N. tabacum*.

the corresponding ones from a previous experiment where tobacco had been grown with [U-$^{13}C_6$]glucose under aseptic conditions (Ettenhuber et al., 2005) (Fig. 3). Moreover, even a preliminary interpretation allows a number of important conclusions. (i) The close agreement of the abundances of the corresponding $\{10XXXX\}_{glc}$, $\{010XXX\}_{glc}$, $\{X010XX\}_{glc}$ and $\{XXXX01\}_{glc}$ pairs from the two different experiments indicates that single-labeled isotopologues were not generated in high amounts from $^{13}CO_2$ in the pulse phase and the subsequent chase phase. (ii) The similar abundances in X-groups comprising multiply labeled isotopologues suggest that the populations of multiply labeled isotopologues are similar in the two experiments; thus, the abundances of the $\{X111XX\}_{glc}$ group suggest similar fractions of the $\{111111\}_{glc}$ isotopologue in the experiments under comparison. (iii) The observation of similar $\{110XXX\}_{glc}$ as well as $\{X011XX\}_{glc}$ abundances comprising the $\{110000\}_{glc}$ and $\{001111\}_{glc}$ isotopologues, respectively, provides evidence for a similar contribution by the transketolase reaction of the pentose phosphate pathway starting from a {111111} isotopologue of hexose phosphate with unlabeled hexose in high excess.

In a prima vista approach, the available data can be best explained by formation of multiply ^{13}C-labeled carbohydrates during the $^{13}CO_2$ pulse phase. Metabolic fragments of this labeled photosynthesis products are then metabolically combined with fragments derived form unlabeled carbohydrates that had already been present prior to the labeling period and/or were generated during the chase phase under $^{12}CO_2$ conditions. The detected isotopologue pattern of glucose then indicates carbohydrate cycling during the chase phase using a mixture of multiply labeled and unlabeled hexose as tracer.

2.3. Isotopologue profiles of amino acids from leaf protein

Using [U-$^{13}C_6$]glucose as a precursor, the labeling patterns of amino acids yield abundant information about quantitative aspects of the metabolic network under study (for a recent example, see Eisenreich et al., 2006). Specifically, the isotopologue patterns in amino acids can be dissected into the patterns of their respective precursors by a retrobiosynthetic approach (Eisenreich et al., 1991, 1993; Szyperski, 1995; for review, see Bacher et al., 1999). Since the basic building blocks of amino acids (for example, acetyl-CoA, pyruvate, phosphoenol pyruvate, oxaloacetate, α-ketoglutarate) constitute principal nodes in the core metabolic network of all organisms, their labeling patterns can be used for a comprehensive analysis of carbon partitioning in the organism under study. To test the validity of this approach for the $^{13}CO_2$ labeling technique, we analysed a set of amino acids from the labeled tobacco plant.

^{13}C NMR signals of alanine, glutamate, and aspartate obtained by hydrolysis of tobacco protein displayed intense ^{13}C-coupling satellite lines indicating the presence of multiply labeled species at significant abundance (for details see Table 2). For example, the signal for ^{13}C-2 of aspartate comprises nine lines of significant intensity (Fig. 4). The complex signal pattern can be deconvoluted on the basis of the known $^{13}C^{13}C$-coupling constants. The abundances for these isotopologue sets can be assessed from the respective signal intensities. For a concise description of the NMR data, the X-group notation that was initially introduced for glucose (Eisenreich et al., 2004b) can be generalised for amino acids and other metabolites. The chemical nature of the compound can be indicated as a subscript to the brace designating the respective compound. For example, the second digit in the isotopologue set $\{XXXX\}_{asp}$designates carbon atom 2 of aspartate according to the IUPAC nomenclature, i.e. the α-carbon atom. In the example displayed in Fig. 4, signals detected for $\{010X\}_{asp}$, $\{110X\}_{asp}$, $\{011X\}_{asp}$ and $\{111X\}_{asp}$ were assigned a molar abundance of 1.48, 0.68, 0.35 and 0.69 mol%, respectively (see also Table 3).

The labeling pattern of glutamate was characterised by two sets of isotopologues comprising three contiguous ^{13}C atoms extending from C-1 to C-3 or C-3 to C-5, i.e. $\{111XX\}_{glu}$ or $\{XX111\}_{glu}$, respectively. Moreover, two isotopologue sets carrying pairs of contiguous ^{13}C atoms, i.e.$\{110XX\}_{glu}$ and $\{XX011\}_{glu}$, are present with significant

Table 2
NMR data of amino acids from *Nicotiana tabacum* proffered with $^{13}CO_2$

	Position	Chemical shift, δ (ppm)	Coupling constants, J_{CC} (Hz)[a]	^{13}C enrichments	
				% ^{13}C[b]	% $^{13}C^{13}C$[c]
Alanine	1	182.9	59.2 (2)	3.1	52.1
	2	59.1	58.8 (1)	3.1	13.6
			33.7 (3)		9.0
			59.9, 33.7 (1, 3)		39.9
	3	25.6	34.2 (2)	3.5[d]	52.9
Aspartate	1	180.7	52.1 (2)	3.2	44.8
	2	54.4	53.8 (1)	3.2[d]	21.2
			36.4 (3)		11.1
			53.2, 35.2 (1, 3)		21.6
	3	43.8	51.5 (4)	3.3	13.0
			35.8 (2)		19.5
			51.5, 35.4 (2, 4)		23.9
	4	182.8	53.4, 4.3 (2, 3)	3.1	45.0
Glutamate	1	183.0	50.9 (2)	3.2	40.6
	2	55.8	52.8 (1)	3.2[d]	22.7
			34.7 (3)		10.9
			52.8, 34.7 (1, 3)		16.4
	3	31.7	34.5 (2 or 4)	3.3	29.3
			35.0, 34.5 (2, 4)		6.9
	4	34.0	51.5 (5)	3.3	38.7
			34.3 (3)		4.0
			52.0, 34.5 (3, 5)		9.5
	5	182.8	50.4 (4)	3.2	47.5

[a] Coupled atoms are given in parentheses.
[b] Absolute ^{13}C abundance of the indexed atom.
[c] Fraction of the indexed coupling pair in the overall signal intensity of the respective ^{13}C NMR signal.
[d] ^{13}C enrichment from the ^{13}C satellites in the ^{1}H NMR spectrum. This value was taken to normalise the relative ^{13}C abundances obtained from the ^{13}C NMR spectrum (for details see Section 5).

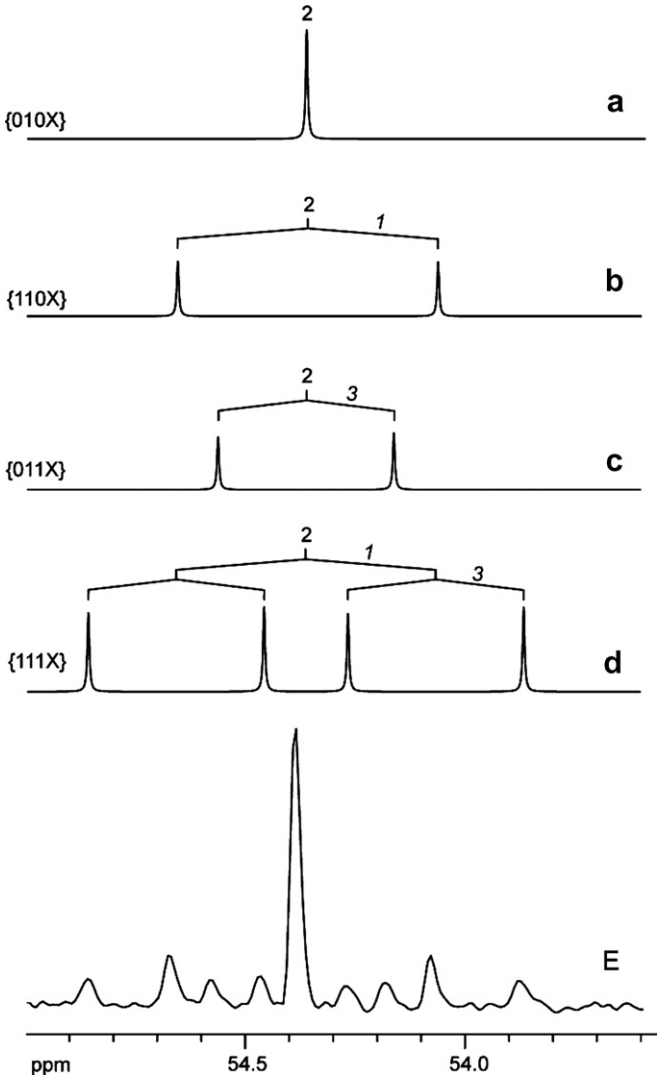

Fig. 4. Numerically simulated NMR signals of the ^{13}C-2 atom in aspartate in different isotopologue sets (X-groups; a–d). The spectroscopically determined NMR signal of C-2 in aspartate from *N. tabacum* pulse-labeled with $^{13}CO_2$ (e). The intensities of the simulated signals were adjusted to show the relative contributions of the isotopologue groups in the biosynthetic sample.

abundance. The labeling pattern of biogenic alanine showed the presence of multiple ^{13}C-enriched species with simultaneous ^{13}C-label at C-1 and C-2, i.e. $\{11X\}_{ala}$, at C-2 and C-3, i.e. $\{X11\}_{ala}$, and C-1, C-2 and C-3, i.e. $\{111\}_{ala}$ (see also Tables 4 and 5).

In order to get quantitative data on additional isotopologue groups of the amino acids under study, we synthesised the *tert*-butyl-di-methyl-silyl derivatives (TBDMS amino acids, Fig. 5) that were subjected to GC/MS analysis (for details, see Section 5). On the basis of the fragmentation patterns shown in Fig. 5, isotopologue abundances were assessed for mass ions comprising all carbon atoms of the original amino acid (fragment b in Fig. 5), mass ions comprising the carbon atoms of the original amino acids without the carboxylic acid atom (fragments c, d and f), and mass ions containing the C-1 and C-2 of the original amino acid (in the case of aspartate) (fragment e). After correcting the detected intensities of the mass peaks using the method described by Lee et al. (1991), molar abundances for carbon isotopologues of the amino acid moiety were calculated (Tables 3–5). As an example, for the fragment b of TBDMS-ala, the normalised $m+1$ peak represents the sum of the {100}-, {010}- and {001}-isotopologues, $m+2$ reflects the sum of the molar abundances of {110}-, {011}-, and {101}-ala, whereas $m+3$ is indicative for the {111}-isotopologue. Fragment c (comprising C-2 and C-3 of ala) affords the molar abundances of {X00}-, {X01, X10}-, and {X11}-groups.

The documentation of these patterns is facilitated by the expanded X-group concept which easily includes molecular fragments observed by mass spectrometry. In that formalism, X designates atom positions that are not present in a given mass spectrometric fragment, while Y designates carbon atoms in the actual fragment. The sum of labeled Y-positions (y) is shown as a superscript integer outside the braces that are used to specify the X-group (e.g. $\{XYY\}^{y}$).

In summary, the abundances of 7 isotopologues/X-groups can be obtained by mass spectrometric analysis of alanine. Notably, the enrichment of $[111]_{ala}$ (i.e.,

Table 3
Isotopologue and X-group abundance in aspartate obtained from protein hydrolysates of tobacco leaves

Fragment	*m/z*	Isotopologue/X-group	mol%
GC/MS			
e	302	{00XX}	94.64
	303	$\{YYXX\}^1$	4.10
	304	{11XX}	1.26
	316	{X000}	91.59
d	317	$\{XYYY\}^1$	6.42
	318	$\{XYYY\}^2$	1.22
	319	{X111}	0.77
	390	{X000}	91.65
c	391	$\{XYYY\}^1$	6.42
	392	$\{XYYY\}^2$	1.06
	393	{X111}	0.87
	418	{0000}	90.42
	419	$\{YYYY\}^1$	6.91
b	420	$\{YYYY\}^2$	1.35
	421	$\{YYYY\}^3$	0.83
	422	{1111}	0.51
Signal	ppm	Isotopologue/X-group	mol%
NMR			
1	180.7	{10XX}	1.76
		{11XX}	1.43
2	54.4	{010X}	1.48
		{110X}	0.68
		{011X}	0.35
		{111X}	0.69
3	43.8	{X010}	1.44
		{X011}	0.43
		{X111}	0.79
		{X110}	0.64
4	182.8	{XX01}	1.71
		{XX11}	1.39

The leaves were cut from plants grown in the presence of $^{13}CO_2$.

Table 4
Isotopologue and X-group abundance in glutamate obtained from protein hydrolysates of tobacco leaves

Fragment	*m/z*	Isotopologue/X-group	mol%
GC/MS			
f	272	{X0000}	90.09
	273	$\{XYYYY\}^1$	6.86
	274	$\{XYYYY\}^2$	2.37
	275	$\{XYYYY\}^3$	0.52
	276	{X1111}	0.15
	330	{X0000}	89.65
	331	$\{XYYYY\}^1$	7.71
d	332	$\{XYYYY\}^2$	2.05
	333	$\{XYYYY\}^3$	0.42
	334	{X1111}	0.18
	404	{X0000}	90.00
	405	$\{XYYYY\}^1$	7.16
c	406	$\{XYYYY\}^2$	1.98
	407	$\{XYYYY\}^3$	0.73
	408	{X1111}	0.13
	433	{00000}	88.29
	434	$\{YYYYY\}^1$	8.41
b	435	$\{YYYYY\}^2$	2.33
	436	$\{YYYYY\}^3$	0.65
	437	$\{YYYYY\}^4$	0.20
	438	{11111}	0.12
Signal	ppm	Isotopologue/X-group	mol%
NMR			
1	183.0	{10XXX}	1.90
		{11XXX}	1.30
2	55.8	{010XX}	1.55
		{110XX}	0.75
		{011XX}	0.36
		{111XX}	0.54
3	31.7	{X010X}	2.10
		{XY1YX}	0.97
		{X111X}	0.23
4	34.0	{XX010}	1.58
		{XX110}	0.13
		{XX011}	1.28
		{XX111}	0.31
5	182.8	{XXX01}	1.68
		{XXX11}	1.52

The leaves were cut from plants grown in the presence of $^{13}CO_2$.

1.28 mol%) was in good agreement with the value obtained by NMR spectroscopy for the same isotopologue (1.24 mol%). For aspartate, the abundances of 12 X-groups were determined from the MS data. Similarly, the abundances of 11 X-groups were obtained for glutamate (Fig. 6).

Although the inclusion of mass spectrometry in the present study significantly increased the number of observables, a sufficient set of linearly independent X-groups was only available for alanine. Linear regression yielded the abundances of all possible carbon isotopologues given in Table 6. For aspartate or glutamate, 2 or 12 additional equations, respectively, would have been required to provide an overdetermined data set for deconvolution. Therefore, the numerical solution becomes unstable in aspartate and glutamate, and the isotopologue abundances for glutamate and aspartate had to be modelled by metabolic simulation.

2.4. Metabolic simulation

The experimentally obtained linear combinations of isotopologues (X-groups in glucose, alanine, aspartate and glutamate) were used as constraints in a computational simulation approach that tries to simulate the sequence of reaction steps which lead to an isotopologue distribution that fits best to the experimental data. In this approach, only reactions which change the isotopologue distribution of a metabolite by breaking or connecting of C–C bonds were considered to be important. Thus all metabolites connected by reversible reactions that do not change the isotopologue distribution were combined into one pool of metabolites. Typically, those compounds are considered to be in rapid equilibrium as for example hexose phosphates, or triose phosphates.

In our simplified model, we use seven pools of central metabolic intermediates (C_3-, C_4-, C_5-, C_6- and C_7- sug-

Table 5
Isotopologue and X-group abundance in alanine obtained from protein hydrolysates of tobacco leaves

Fragment	*m/z*	Isotopologue/X-group	mol%
GC/MS			
c	232	{X00}	93.69
	233	{XYY}[1]	4.31
	234	{X11}	2.00
	158	{X00}	94.10
d	159	{XYY}[1]	3.96
	160	{X11}	1.94
	260	{000}	92.45
b	261	{YYY}[1]	4.84
	262	{YYY}[2]	1.42
	263	{111}	1.28
Signal	ppm	Isotopologue/X-group	mol%
NMR			
1	182.9	{10X}	1.49
		{11X}	1.61
2	59.1	{010}	1.16
		{110}	0.42
		{011}	0.28
		{111}	1.24
3	25.6	{X01}	1.90
		{X11}	1.85

The leaves were cut from plants grown in the presence of $^{13}CO_2$.

ars/sugar phosphates, oxaloacetate and 2-ketoglutarate), one fixed pool for carbon dioxide and three additional pools for the amino acids alanine, aspartate and glutamate which are connected to their precursor pools (C_3-sugars including pyruvate, oxalacetate and α-ketoglutarate, respectively) by exchange reactions. Every pool is represented by a vector of 2^n isotopologues (n = number of C-atoms). In an attempt to simulate the complex non-steady state situation in the $^{13}CO_2$ experiment, the calculation starts with the natural abundance distribution of the 64 isotopologues in the pool of C_6 sugars and a randomly chosen sequence of reaction steps which shuffles increments of isotopologues between the pools. In this period, CO_2 at a given ^{13}C enrichment (which is known from the experiment, i.e. 88% ^{13}C in the present example) is incorporated by the RUBISCO reaction. As a consequence, multiple ^{13}C-labeled isotopologues originate from multiply labeled triose phosphate by the reactions of the network. In the second mode of the calculation, the $^{13}CO_2$ concentration is fixed at 1.11% in order to simulate the conditions of the chase period. The timing of the switch between the two modes is also optimised by the genetic algorithm. Typically, this switch occurs after 20–30% of all reaction steps in the calculation.

The model includes 21 reactions: glycolysis/glucogenesis (GLY, NEO), 4 transketolase reactions (TK55, TK37, TK54, TK63), 2 transaldolase reactions (TA63, TA37), the oxidative decarboxylation of the pentose phosphate pathway (PPO), 2 reactions of the tricarboxylic acid cycle (TCA1, TCA2), pyruvate carboxylase (OXA) and phosphoenolpyruvate carboxykinase (OX3), which connect the C_3 and the oxaloacetate pool, the aldolase (A34) and the reaction catalysed by RUBISCO (RUB) of the Calvin cycle, and six additional transamination reactions between the amino acids and their precursors.

Because the isotopologues of a given metabolite or metabolite pool are represented by binary numbers between 0 and 2^n, the mechanistic rules of isotope redistribution in each reaction step can be easily translated into binary language using the bitwise shift operators (≪,≫) together with the bitwise AND- and OR-operators (&,|) of the C/C++ language. The binary rules given in Table 7 are used to calculate the vector-indices (=binary representations) j of the product isotopologues of a reaction from the vector-indices a and b of the reactant isotopologues (for more details about the used atom mapping and two representative examples of the metabolic rules used in this study, see supplementary data).

After each reaction, the isotopologue distributions of the pools are recalculated. At the end of each sequence, the simulated isotopologue distributions are converted into the corresponding X-groups of the analysed metabolites by matrix multiplication and compared with the experimental values. The resulting rms deviation is used as a fitness criterion for a genetic algorithm to optimise the reaction sequence. The flow chart in Fig. 7 illustrates the concept of the simulation approach. In Fig. 6, the spectroscopically determined X-group abundances of alanine, aspartate, glutamate and glucose are compared with the simulated datasets. X-groups derived from mass spectroscopy are shown in blue, X-groups from NMR spectroscopy in green. In most cases, the simulated X-groups (shown in red) gave good agreement with the experimental ones.

On this basis, the simulated isotopologue distributions of alanine (Table 6), aspartate and glutamate (Table 8) serve as a good approximation of the real isotopologue pattern in these amino acids. The simulated isotopologue set of alanine was in good agreement with that from the experimental X-groups by numerical deconvolution, again demonstrating the validity of the experimental approach.

The metabolic simulation also results in the assessment of the relative flux contributions of all metabolic reactions implemented in our model (Fig. 8). The arrows in the figure are scaled by the mean relative contributions of the corresponding reaction paths in the simulation. Numeric values with their standard deviations are given in Table 7. The data indicate metabolic flux dominated by reactions from the Calvin cycle (RUBISCO, aldolase, transketolase, transaldolase, and gluconeogenesis) and only a minor contribution by the tricarboxylic acid cycle.

To check the stability of the solution, eight populations with randomly generated start sequences were optimised by the genetic algorithm. For many reaction modes of the carbohydrate metabolism the standard deviations were below 30% (cf. Table 7). Notably, the contributions of the reactions in the citrate cycle were less well defined, as shown by the higher standard deviations.

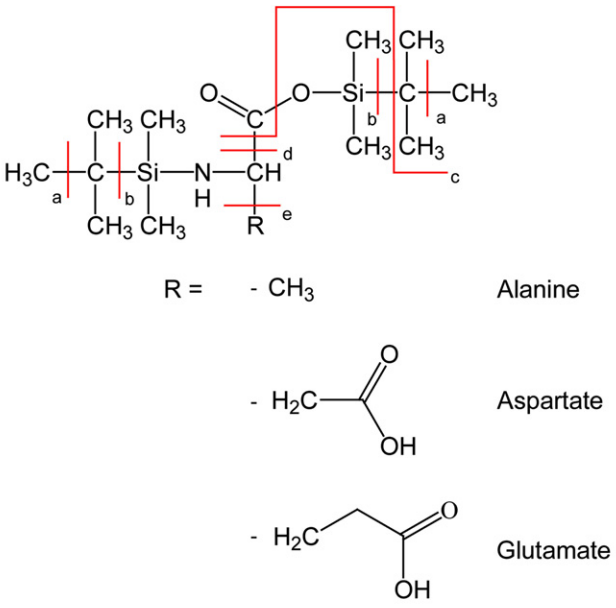

Resulting fragments:
a = $(M - 15)^+$ and methyl group
b = $(M - 57)^+$ and *tert*-butyl group
c = $(M - 85)^+$ and *tert*-butyl group including CO
d = $(M - 159)^+$ and C(O)-TBDMS ion
e = $(f302)^+$ double silylated C_1-C_2 fragment and $(sc)^+$ side chain
f = $(M - 159 - 57 - 1)^+$, C(O)-TBDMS ion , *tert*-butyl group and proton

Amino Acid	$(M - 15)^+$	$(M - 57)^+$	$(M - 85)^+$	$(M - 159)^+$	$(f302)^+$	$(sc)^+$	$(M - 159 - 57 - 1)^+$
Alanine	- {YYY}	260 {YYY}	232 {XY}	- {XY}	- {YYX}	- {XXY}	- {XYY}
Aspartate	- {YYYY}	418 {YYYY}	390 {XYYY}	316 {XYYY}	302 {YYXX}	- {XXYY}	- {XYYY}
Glutamate	- {YYYYY}	432 {YYYYY}	404 {XYYYY}	330 {XYYYY}	- {YYXXX}	- {XXYYY}	272 {XYYYY}

Fig. 5. TBDMS derivatives of the amino acids alanine, aspartate, and glutamate. The fragmentation pattern and the respective mass ions are indicated. The respective fragments are also indicated in Tables 3–5.

It should be noted that the calculated flux pattern can only be taken as a simplified model for the real metabolic fluxes in the living plant. For example, the model does not involve potential "zero-flux" reaction modes of the pentose phosphate pathway reported recently (Van Winden et al., 2001). It should also be noted that the results reflect the overall flux pattern during several light/dark cycles.

2.5. Isotopologue profile of nicotine

Most ^{13}C NMR signals of biosynthetic nicotine (with the exception of the *N*-methyl group of nicotine) appeared as multiplets due to $^{13}C^{13}C$ coupling (Fig. 9). This shows that multiple isotopologues were formed with significant abundance. The ^{13}C multiplets display different levels of complexity due to the presence of molecular species carrying one, two, or three contiguous ^{13}C atoms and/or by the presence of multiple isotopologues.

The abundances of individual isotopologue sets were assessed quantitatively from the NMR signal intensities, as described above for amino acids. Briefly, the combined integrals of the coupling patterns characteristic for isotopologue groups (i.e. comprising one or multiple ^{13}C-atoms in a structural moiety) are referenced to the global signal intensity of the corresponding carbon atom (Table 9). The abundances of observed isotopologue groups (shown as mol%) in nicotine (compound **1**) are summarised in Fig. 10. The isotopologue profile shows beyond doubt that multiply ^{13}C-labeled molecular species have been generated at abundances exceeding the respective isotopologue abundances by 1–3 orders of magnitude as compared with nicotine at a stochastic distribution of the ^{13}C-label (see also Table 10).

Nicotine (**1**) has been shown earlier to be assembled from amino acid precursors in the root system of tobacco wherefrom it is transported to the leaves *via* the xylem (Dawson, 1941; Mizusaki et al., 1973). The pyrimidine ring of the alkaloid is derived from nicotinic acid (**9**) which is biosynthesised in plants from glyceraldehyde phosphate (**7**) and aspartate (**8**) (for reviews see Leete, 1992; Bush et al., 1999; Katoh and Hashimoto, 2004; Katoh et al., 2005). Although there was a long dispute about the symmetry of the precursors used for the synthesis of the pyrrolidine ring (Liebman et al., 1967; Rueppel et al., 1974; Leete, 1976), it is now generally accepted that the pyrrolidine ring is

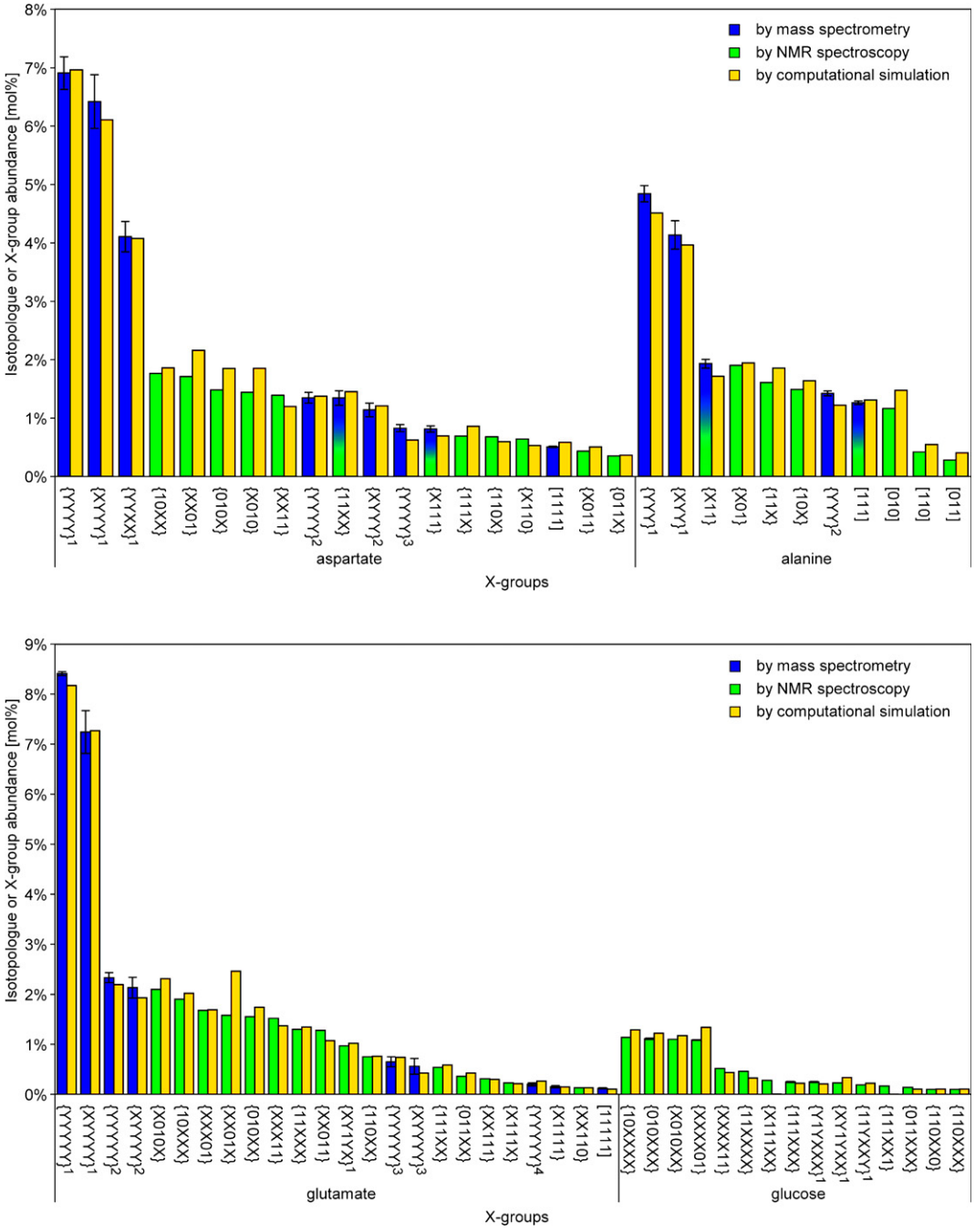

Fig. 6. Comparison of X-group abundances derived from mass spectroscopy, (blue) NMR spectroscopy (green) and metabolic simulation (orange). The standard deviation of several independent measurements from mass spectroscopy are shown as error bars. (For interpretation to color in the figure, the reader is referred to the web version of this article.)

biosynthesised from ornithine (**3**) *via* the symmetrical putrescine (**4**) and the *N*-methyl-2-pyrrolidinium ion (**5**) by a sequence of decarboxylation, reductive amination and oxidative deamination (Dewey et al., 1955; Leete, 1958; Leete, 1967; Leete and McDonell, 1981).

A prediction of the labeling pattern of nicotine based on the labeling patterns of the precursor amino acids is shown in Fig. 10. Since the biosynthesis of the pyrrolidine ring proceeds via the symmetrical putrescine (**4**) as an intermediate, the apparent labeling patterns of the putrescine-derived metabolites are also characterised by symmetrisation. As a consequence, the abundances of the [6,7-$^{13}C_2$]- and the [8,9-$^{13}C_2$]-isotopologues of nicotine should be identical. Indeed, this is observed for nicotine in our $^{13}CO_2$ experiment (Table 10, Fig. 10). This is in contrast to the results obtained by the earlier $^{13}CO_2$ study on nicotine biosynthesis where unsymmetrical label distribution was deduced from the NMR data (Hutchinson et al., 1976; Nakane and Hutchinson, 1978).

The comparison of the predicted isotopologue composition (on the basis of the labeling patterns of the precursor units derived from amino acid data) and the observed

Table 6
Isotopologue composition of alanine obtained from protein hydrolysates of $^{13}CO_2$-labeled tobacco leaves

Isotopologue	Deconvolution (mol%)	Simulation (mol%)
000	92.47	92.96
100	1.42	1.36
010	1.39	1.48
001	1.98	1.67
110	0.53	0.54
011	0.60	0.40
101	0.15	0.27
111	1.26	1.31

The data were calculated by numerical deconvolution of the X-group abundances obtained by NMR spectroscopy and mass spectrometry or metabolic simulation.

isotopologue composition of nicotine shows qualitatively similar labeling patterns (Fig. 10). Clearly, the retrobiosynthetic approach corroborates the well-known biosynthetic dissection of the alkaloid. In quantitative terms, however, the level of labeling is approximately 10 times higher in the amino acids hydrolysed from leaf protein than in nicotine also isolated from leaves. The apparent dilution of the label in nicotine as compared to amino acids is not surprising in light of topological and dynamic aspects of nicotine biosynthesis. The transport of biosynthetic amino acids and triose phosphate serving as nicotine precursors from the leaves to the root system and the re-export of the alkaloid biosynthesised in the roots to the leaf compartment is expected to result in dilution of the label by contributions from biomass that had been formed prior to the $^{13}CO_2$labeling pulse. However, even with this qualification, the detected isotopologue profile of nicotine enables the unequivocal reconstruction of the building blocks used in the biosynthetic process.

3. Discussion

This study was designed to check the suitability of $^{13}CO_2$ as a tracer for biosynthetic studies using advanced analytical tools such as high-resolution NMR spectroscopy, retrobiosynthetic analysis and computational modelling. Tobacco was selected as a model system since the biosynthetic pathways of nicotine, amino acids and glucose are known in considerable detail. Thus, the biosynthesis of the alkaloid can be treated as a test case to evaluate the resolving power of the $^{13}CO_2$ labeling method as a tool for retrobiosynthetic studies in plants.

Our data provide clear evidence for the formation of multiply ^{13}C-labeled isotopologues of a variety of biomolecules as documented by the complex isotopologue patterns of glucose, nicotine and various proteinogenic amino acids. Most importantly, however, the observed labeling pattern of nicotine is qualitatively similar to that predicted from the observed labeling patterns of the precursor amino acids *via* the known biosynthetic pathway, although the isotope excess in nicotine is only about 10% as compared with the precursor amino acids.

Using $^{13}CO_2$ as a precursor, the isotope label is expected to be diverted to all departments of the plant metabolom comprising thousands of low molecular weight compounds. Moreover, the labeled metabolite species generated in this approach are complex mixtures of numerous isotopologues. This is in stark contrast to more conventional labeling techniques where the label is proffered in the form of a single isotopologue of a single, structurally complex metabolite.

In order to characterise certain aspects of the $^{13}CO_2$ labeling strategy, a comparison with labeling strategies using [U-$^{13}C_6$]glucose is helpful (Eisenreich et al., 2004b; Ettenhuber et al., 2005). Similar to label from $^{13}CO_2$, label from ^{13}C-glucose is expected to be diverted to all compartments of the plant metabolom. In order to generate the required starting conditions characterised by a non-random distribution of ^{13}C, the universally labeled carbohydrate is typically applied together with a large excess of unlabeled glucose. Catabolism of the labeled carbohydrate affords ^{13}C-labeled fragments that can subsequently be used by anabolic pathways where they can recombine with other modules. Due to the large excess of unlabeled glucose proffered together with the universally labeled glucose, the labeled catabolites will predominantly form novel carbon/carbon bonds with metabolic fragments from unlabeled precursor molecules; hence, the anabolic reactions will not result in the formation of novel adjacent $^{13}C^{13}C$ pairs and the metabolic remodelling will almost exclusively result in the breakage rather than the formation of $^{13}C^{13}C$ bonds. In summary, this is conducive to a redistribution of the isotope label and a concomitant increase in the isotopologue pattern.

In contrast to the glucose labeling study where the multiply labeled tracer is proffered with a large excess of unlabeled material, $^{13}CO_2$ is applied in isotopically pure form. The labeling pulse is therefore expected to result in the photosynthetic generation of a mixture of multiply ^{13}C-labeled monosaccharide phosphates. The generation of unlabeled carbohydrates by the photosynthetic assimilation of CO_2 with natural ^{13}C abundance (1.11%) in the subsequent chase period can be expected to provide unlabeled molecular species that enable metabolic processes conducive to the redistribution of ^{13}C in a way that is similar to the relaxation process described above for the experiment with ^{13}C-labeled glucose. Indeed, similar relative abundances of X-groups in glucose from the $^{13}CO_2$ experiment and the earlier experiment with [U-$^{13}C_6$]glucose (Ettenhuber et al., 2005) support this conclusion.

The experimental conditions of the pulse/chase experiment can be varied over a wide range *via* trimming of the pulse and chase periods and by the lighting conditions. As a general rule, conditions should be used that minimise $^{12}CO_2$ formation during the pulse period since metabolically generated $^{12}CO_2$ dilutes the proffered $^{13}CO_2$; fortunately, the extent of $^{12}CO_2$ formation can be easily

Table 7
Binary rules used in the computational simulation (for details, see also supplemental material)

Reaction		Relative contribution (%)	Binary rules		Isotopologue	
					a	b
GLY	$C_6 \rightarrow 2C_3$	4.8 ± 2.1	$j = (a \gg 3)\&7$	$j = ((a \ll 2)\&4)\|(a\&2)\|((a \gg 2)\&1)$	C_6	
TK55	$2C_5 \rightarrow C_3 + S7P$	2.6 ± 0.8	$j = (a \gg 2)\&7$	$j = (a\&3)\|((b \ll 2)\&124)$	C_5	C_5
TK37	$C_3 + S7P \rightarrow 2C_5$	9.5 ± 1.4	$j = (b \gg 2)\&31$	$j = (b\&3)\|((a \ll 2)\&28)$	C_3	S7P
TK54	$C_5 + E4P \rightarrow C_6 + C_3$	2.4 ± 1.2	$j = (a \gg 2)\&7$	$j = (a\&3)\|((b \ll 2)\&60)$	C_5	E4P
TK63	$C_6 + C_3 \rightarrow C_5 + E4P$	10.7 ± 1.8	$j = (a \gg 2)\&15$	$j = (a\&3)\|((b \ll 2)\&28)$	C_6	C_3
TA37	$C_3 + S7P \rightarrow C_6 + E4P$	2.5 ± 1.4	$j = (b \gg 3)\&15$	$j = (b\&7)\|((a \ll 3)\&56)$	C_3	S7P
TA64	$C_6 + E4P \rightarrow C_3 + S7P$	1.4 ± 0.4	$j = (a \gg 3)\&7$	$j = (a\&7)\|((b \ll 3)\&120)$	C_6	E4P
OXA	$C_3 + CO_2 \rightarrow OA$	2.8 ± 2.3	$j = a\&7$	$j = (a\&7)\|8$	C_3	
TCA2	$KG \rightarrow OA + CO_2$	0.7 ± 0.5	$j = (a \gg 1)\&15$	$j = ((a \gg 4)\&1)\|((a \gg 2)\&2)\|(a\&4)\|((a \ll 2)\&8)$	KG	
RUB	$C_5 + CO_2 \rightarrow 2C_3$	24.8 ± 4.5	$j = (a \gg 2)\&7$	$j = (a\&2)\|((a \ll 2)\&4)\|1$ *or* $j = (a\&2)\|((a \ll 2)\&4)$	C_5	
PPO	$C_6 \rightarrow C_5 + CO_2$	3.8 ± 2.5	$j = (a \gg 1)\&31$		C_6	
OX3	$OA \rightarrow C_3 + CO_2$	1.8 ± 1.1	$j = a\&7$		OA	
NEO	$2C_3 \rightarrow C_6$	15.5 ± 1.3	$j = ((a \gg 2)\&1)\|(a\&2)\|((a \ll 2)\&4)\|\ ((b \ll 3)\&56)$		C_3	C_3
TCA1	$C_3 + OA \rightarrow KG + 2CO_2$	1.0 ± 0.6	$j = ((b \gg 3)\&1)\|((b \gg 1)\&2)\|((b \ll 1)\&4)\|\ ((a \ll 1)\&8)\|((a \ll 3)\&16)$		C_3	OA
A34	$C_3 + E4P \rightarrow S7P$	9.0 ± 1.7	$j = ((b \ll 3)\&120)\|(a\&2)\|((a \gg 2)\&1)\|\ ((a \ll 2)\&4)$		C_3	E4P
Six more reactions	Ala ↔ C_3	0.3–2.2	$j = a$		C_3	
	Asp ↔ OA				OA	
	Glu ↔ KG				KG	

The rules are based on established textbook knowledge about metabolic transformations in plants. Mean values for the relative contributions are given on the basis of eight independent calculations. Reactions due to GLY, glycolysis; TK, transketolase; TA, transaldolase; OXA, pyruvate carboxylase; TCA, tricarboxylic acid cycle; RUB, rubisco; PPO, oxidative pentose phosphate pathway; OX3, phosphoenolpyruvate carboxykinase; NEO, gluconeogenesis; A, aldolase. The metabolic pools are indicated by C_6, hexose pool; C_5, pentose pool; C_3, triose pool; S7P sedoheptulose 7-phosphate; E4P, erythrose 4-phosphate; OA, oxaloacetate; KG, α-ketoglutarate. j is a binary index of a reaction product isotopologue; a and b are binary indices of reactant isotopologues.

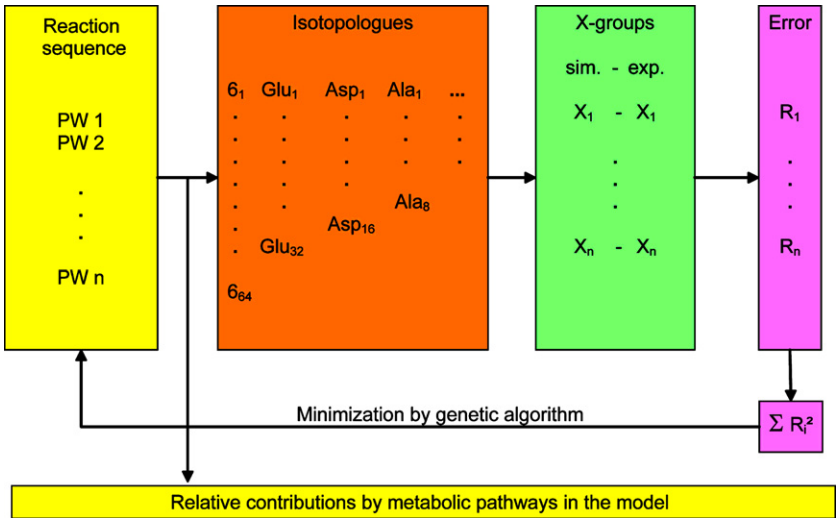

Fig. 7. Flow chart of the metabolic simulation in this study. A reaction sequence of metabolic operators representing different pathways (PW1...PW*n*) generates distinct isotopologue distributions in various metabolic pools. The calculated isotopologues of glucose (6), glutamate (Glu), aspartate (Asp), and alanine (Ala) are converted into X-groups and compared with the experimental values. The rms deviation is used as a fitness criterion using a genetic algorithm to optimise the initially randomly chosen reaction sequence.

Table 8
Isotopologue composition of aspartate and glutamate obtained from protein hydrolysates of $^{13}CO_2$-labeled tobacco leaves

Aspartate		Glutamate	
Isotopologue	Simulation (mol%)	Isotopologue	Simulation (mol%)
0000	90.46	00000	88.52
1000	1.53	10000	1.70
0100	1.79	01000	1.63
0010	1.77	00100	2.10
0001	1.87	00010	1.29
1100	0.48	00001	1.45
1010	0.09	11000	0.59
1001	0.12	10100	0.14
0110	0.26	10010	0.03
0101	0.05	10001	0.03
0011	0.38	01100	0.34
1110	0.27	01010	0.03
1101	0.12	01001	0.03
1011	0.12	00110	0.05
0111	0.10	00101	0.05
1111	0.59	00011	0.88
		11100	0.40
		11010	0.03
		11001	0.03
		10110	0.01
		10101	0.01
		10011	0.04
		01110	0.02
		01011	0.05
		01101	0.02
		00111	0.10
		11110	0.04
		11101	0.04
		11011	0.10
		10111	0.03
		01111	0.05
		11111	0.10

The data were obtained by metabolic simulation (for details see text).

assessed by simultaneous recording of $^{13}CO_2$ as well as $^{12}CO_2$ throughout the experimental period.

Various strategies can be used for the application of ^{13}C-labeled organic tracer compounds to plant tissues or cells, such as (i) working with plant cell suspension cultures, (ii) with cut plant segments or (iii) with aseptically grown intact plants. Cell cultures are only available for a restricted range of species; moreover, secondary metabolites produced by the intact plant are not always produced in significant and experimentally sufficient amounts by cultured cells. Similarly, the use of cut segments is not always conducive to the *de novo* formation of labeled metabolic products in amounts that are sufficient for analysis; notably, unsuccessful experimental designs will typically not enter the public domain. The strategy using aseptically grown whole plants depends on the availability of appropriate plant material and on the ability of the proffered precursor to be taken up efficiently *via* the root system. On the other hand, the ^{13}C pulse-labeling technique described in this study can be used with all photosynthetic plants without any qualification. Even in cases of tall species where full size plants are too large for $^{13}CO_2$ incubation chambers, the use of seedling or specimens that have not yet reached their full size remains possible.

4. Conclusion

The $^{13}CO_2$ labeling strategy results in the photosynthetic generation of a multiply ^{13}C-labeled population of carbohydrate phosphates. This population of multiply ^{13}C-labeled isotopologues is diluted with unlabeled carbohydrates generated during the chase period. The resulting

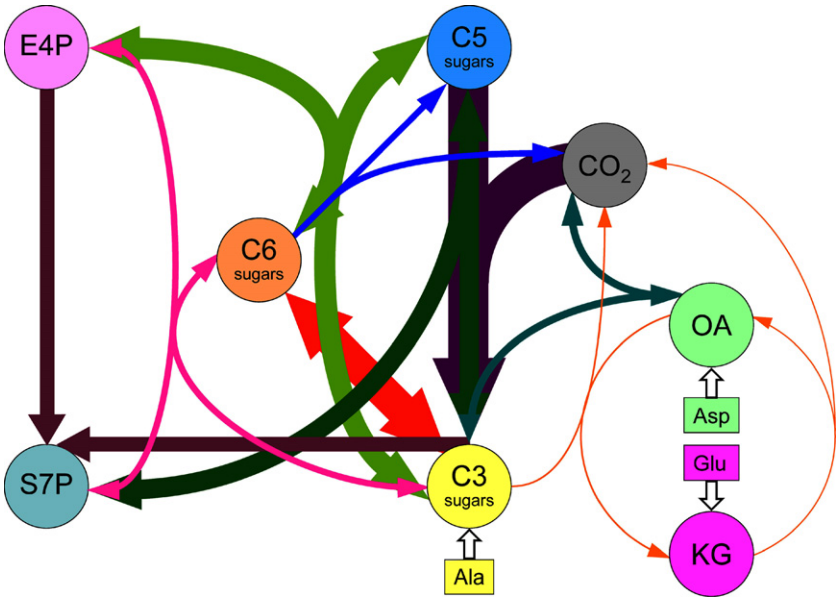

Fig. 8. Metabolic network model used for simulation in this study. The network contains seven central metabolite pools and additional pools for CO_2 and amino acids. The pools are connected by 15 reactions redistributing the carbon skeleton and, therefore, the isotopic state of the reactants. Mean values for the relative contributions from eight independent simulation runs are indicated by the arrow width (cf. also Table 7).

mixture affords non-random mosaics of isotopologues by metabolic processing during the chase period. The specific isotopologue profiles reflect the biosynthetic history of each metabolite under study and can be used to identify the building blocks in the biosynthesis of natural products. The data can also be integrated into computational analyses providing relative contributions of the reaction pathways in the respective non-steady state model. It is obvious that the experimental approach can be used in general for the assessment of metabolite partitioning in unperturbed plants.

5. Experimental

5.1. $^{13}CO_2$ labeling

A growing plant of *Nicotiana tabacum* with a height of about 40 cm was placed in a closed plant growth chamber (BIOBOX, GWS, Berlin). During an adaptation light period of 6 h at 26 °C and a dark period of 12 h at 22 °C and 66% humidity, the plant was exposed to synthetic air containing 20.5% oxygen and 700 ppm CO_2. Prior to the labeling period, the chamber was flushed with synthetic air containing only oxygen and nitrogen. Then, the plant was exposed to synthetic air containing 600 ppm $^{13}CO_2$ (Campro Scientific, Berlin, Germany, >99% ^{13}C abundance) as the only carbon source and was illuminated with white light (about 20,000 lx) at 26 °C for 5 h. Subsequently, the plant was kept for 18 h in the dark and was then allowed to grow under standard greenhouse conditions at ambient temperature for 10 days. Biomass was then harvested and lyophilised.

5.2. Isolation of nicotine

Lyophilised leaves (100 g) were homogenised and extracted with 700 ml of methanol. The extract was filtered and evaporated to a volume of 5 ml under reduced pressure. The solution was extracted with 500 ml of diethyl ether. The aqueous phase was adjusted to pH 11 by the addition of 1 ml of 25% ammonia and was then extracted with 300 ml of diethyl ether. The organic phase was concentrated to 3 ml under reduced pressure. The solution was extracted with 0.5 ml of $CDCl_3$. The $CDCl_3$ solution was analysed by NMR spectroscopy.

5.3. Isolation of amino acids

The residual biomass was hydrolysed as described earlier, and amino acids were isolated by published procedures (Eisenreich et al., 1991).

5.4. Isolation of glucose

Tobacco leaves (5 g wet weight) were frosen with liquid nitrogen, pulverised and extracted with 100 ml of water. The mixture was centrifuged, and 100 ml of methanol were added. The solution was filtered and evaporated to dryness under reduced pressure. The residue was dissolved in 3 ml of water and adjusted to pH 11 by the addition of 1 ml of 25% ammonia. The solution was applied to a Boronate Gel column (Bio-Rad Laboratories GmbH, Munich, Germany) which was washed with 0.25% ammonia until all colored components were removed. The column was then developed with 1% formic acid. Fractions containing glucose were combined and evaporated to a volume of 5 ml

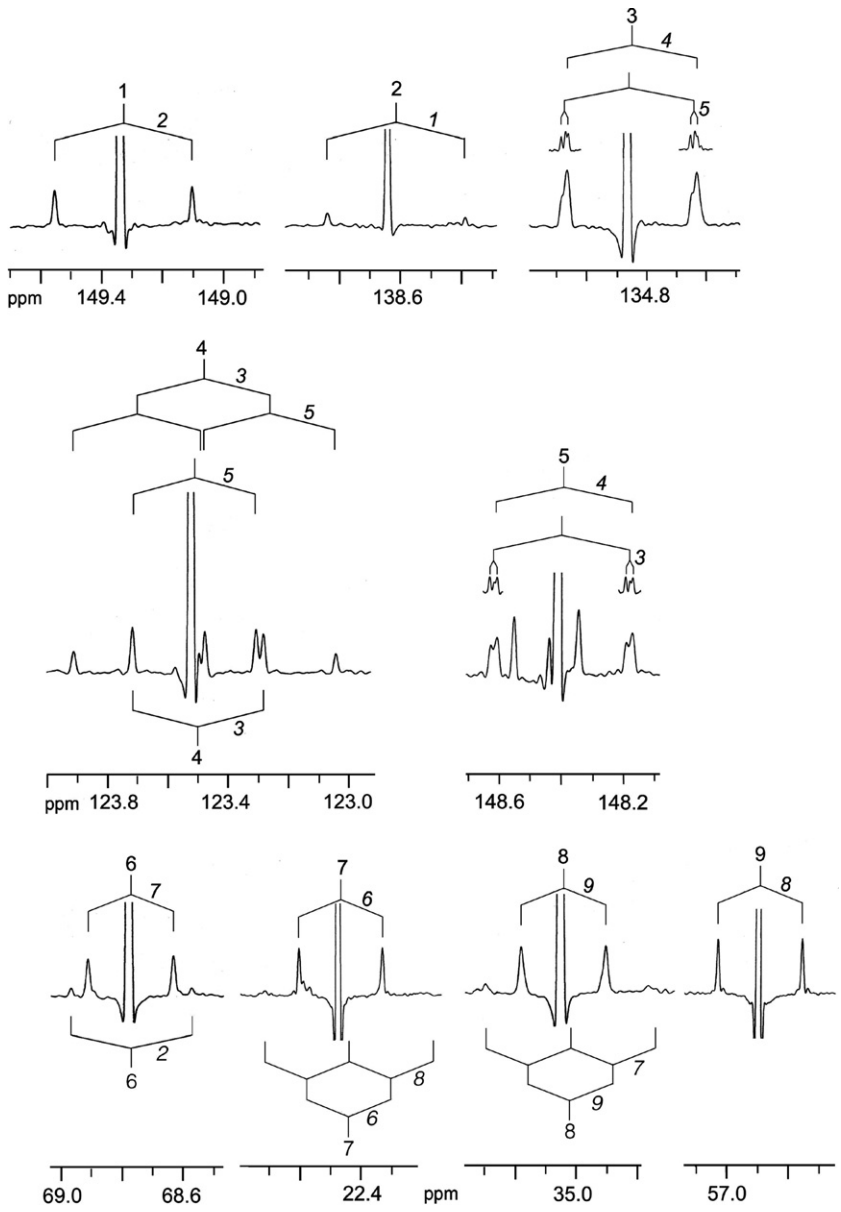

Fig. 9. ^{13}C NMR signals of nicotine from *N. tabacum* pulse-labeled with $^{13}CO_2$. ^{13}C-coupling patterns are indicated.

under reduced pressure. The solution was applied to a Dowex 1 × 8 column (Serva Electropheresis GmbH, Heidelberg, Germany) which was eluted with water. Fractions were combined and evaporated to a volume of 5 ml under reduced pressure. Aliquots were applied to a Luna NH_4 HPLC column (Phenomenex, Torrance CA, USA) which was developed with acetonitril/water (85:15, v/v) (40 °C; flow rate, 20 ml/min). The effluent was monitored refractometrically using a GAT LCD 201 differential refractometer from Gamma Analysen Technik GmbH, Bremerhaven, Germany. The retention volume of glucose was 480 ml. Fractions were combined and lyophilised.

5.5. Isotopologue abundances by NMR spectroscopy

NMR spectra were recorded at 27 °C using a DRX 500 spectrometer (Bruker Instruments, Karlsruhe, Germany). Nicotine was measured in $CDCl_3$ as solvent. Published ^{13}C NMR signal assignments of nicotine (Breitmaier et al., 1979) were confirmed by two-dimensional INADEQUATE experiments. Aspartate, glutamate and alanine were measured in 0.1 M DCl as solvent. Signal assignments were taken from Eisenreich et al. (1993). Glucose was dissolved in D_2O. Signal assignments, coupling constants and isotope shifts were taken from Eisenreich et al. (2004b).

Relative ^{13}C abundance was determined by comparing the signal intensities of the biosynthetic samples with the signals of samples with natural ^{13}C abundance measured under identical spectroscopic conditions (Eisenreich and Bacher, 2000). Absolute ^{13}C abundances were determined *via* the ^{13}C-coupled satellites in ^{1}H NMR spectra (Eisenreich and Bacher, 2000). The relative ^{13}C abundances were then referenced to the absolute values (% ^{13}C in Tables 2 and 9).

Table 9
NMR data of nicotine from *Nicotiana tabacum* proffered with $^{13}CO_2$

Position	Chemical shift, δ (ppm)	Coupling constant[a], J_{CC} (Hz)	^{13}C enrichments	
			% ^{13}C[b]	% $^{13}C^{13}C$[c]
1	149.5	56.8 (2)	1.2	10.0
2	138.8	56.8 (1)	1.2	13.8
3	135.0	54.6, 2.4 (4, 5)	1.3[d]	16.8
4	123.7	54.8 (3, 5)	1.3	9.9
		54.8, 54.7 (3, 5)		11.3
5	148.6	54.8, 2.4 (3, 4)	1.5	14.7
6	69.0	35.1 (7)	1.2	9.8
		49.7 (2)		1.6
7	22.7	34.3 (6)	1.2	12.4
		35.4, 35.3 (6, 8)		3.4
8	35.2	34.3 (9)	1.2	10.8
		34.3, 35.3 (7, 9)		2.8
9	57.1	34.4 (8)	1.3	10.7
10	40.4		1.3	

[a] Coupled atoms are given in parentheses.
[b] Absolute ^{13}C enrichment of the indexed atom.
[c] Fraction of the indexed coupling pair in the overall signal intensity of the respective ^{13}C NMR signal.
[d] ^{13}C enrichment from the ^{13}C satellites in the ^{1}H NMR spectrum. This value was taken to normalise the relative ^{13}C abundances obtained from the ^{13}C NMR spectrum (for details see Section 5).

Multiple-labeled isotopologues displaying $^{13}C^{13}C$ coupling were quantified from the corresponding satellite signals in the ^{13}C NMR spectra (Eisenreich and Bacher, 2000). The integral of each respective satellite pair was then referenced to the total signal integrals of a given carbon atom (%$^{13}C^{13}C$ in Tables 2 and 9). From the overall ^{13}C abundances, the molar contribution of a specific isotopologue or an isotopologue group (X-group) was then assessed (Tables 1, 3–5 and 10).

5.6. Isotopologue abundances by GC/MS

tert-Butyl-di-methylsilyl amino acids (TBDMS amino acids) were prepared according to Dauner and Sauer (2000). Aliquots (about 10 μg) of each amino acid under study were dissolved in 50 μl of freshly distilled tetrahydrofuran. *N*-(*tert*-butyldimethylsilyl)-*N*-methyl-trifluoroacetamide containing 1% *tert*-butyldimethyl-silylchloride (50 μl) was added. The mixture was kept at 85 °C for 60 min and was used for GC–MS analysis without further work-up.

GC/MS analyses were performed on a GC-17A Gas Chromatograph (Shimadzu, Duisburg, Germany) equipped with a fused silica capillary column (Equity TM-5; 30 m × 0.25 mm × 0.25 μm film thickness; SUPELCO, Bellafonte, PA) coupled to a QP-5000 mass selective detector (Shimadzu, Duisburg, Germany) working with electron impact (EI) ionisation at 70 eV. An aliquot (1 μl) of a solution containing TBDMS amino acids was injected in 1:5 or 1:10 split mode at the interface temperature of 260 °C and a helium inlet pressure of 70 kPa. The column was developed at 150 °C for 3 min and then with a temperature gradient of 10 °C/min to a final temperature of 260 °C that was held for 3 min. The retention times of TBDMS-alanine, TBDMS-aspartate and TBDMS-glutamate were 6.7 min, 13.0 min and 14.0 min, respectively.

Data were collected using the Class 5000 software (Shimadzu, Duisburg, Germany). Selected ion monitoring experiments were carried out on the fragments summarised in Fig. 5. Selected ion monitoring data were acquired using a 0.3 s sampling rate. Each sample was analysed at least five times.

Data evaluation was performed using Microsoft Excel Software. Statistical analysis of the tracer data was done to determine mean, standard deviation and intersample variance. Theoretical isotope ratio and numerical deconvolution of the data were based on a 3-step procedure published by Lee et al. (1991): (i) determination of the 'TBDMS-derivative' spectrum for the TBDMS amino acids, (ii) determination of the mass isotopomer distribution of the labeled TBDMS amino acids, (iii) correction for incorporation of ^{13}C from natural abundance. This results in molar excess of carbon isotopologue groups (X-groups) or isotopologues of the amino acid skeleton.

5.7. Simulation

Simulation of metabolic pathways was done in a non-steady state one-compartment model with 21 reactions and 11 pools of metabolites (for details, see also supplementary data). Metabolites connected through a rapid equilibrium of reversible reactions without skeletal rearrangement of carbon atoms were treated as a single pool. For example, the pool of C_6-sugars represents glucose, glucose 6-phosphate, fructose 6-phosphate and fructose 1,6-biphosphate. Similarly, ribose 5-phosphate, ribulose 5-phosphate, and xylulose 5-phosphate are summarised in a C_5-pool. Glyceraldehyde 3-phosphate, dihydroxyacetone 3-phosphate, phosphoglycerate, phosphoenolpyruvate and pyruvate build up the C_3-pool. The isotopologue distribution of acetyl-CoA is represented by the carbon atoms C-2 and C-3 of the C_3-pool in our model.

Starting with the natural abundance distribution of glucose in the C_6-pool, sequences of metabolic operators (reactions) shuffle increments of the isotopologues from one or two pools to one or more product-pools according to the known rules of breaking and reconnecting carbon–carbon bonds by the various metabolic pathways. ^{13}C incorporation is simulated by the reaction catalysed by RUBISCO converting one molecule each from the C_5-pool and the CO_2-pool into two C_3-pool metabolites. The ^{13}C enrichment in the CO_2-pool is restricted to a narrow interval around the experimentally measured concentration of $^{13}CO_2$ in the chamber during the pulse phase and switched to 1.11% during the chase phase. The timing of this switch is also optimised during the simulation.

After simulation of a complete sequence of reactions, X-groups are calculated from the isotopologue distribution

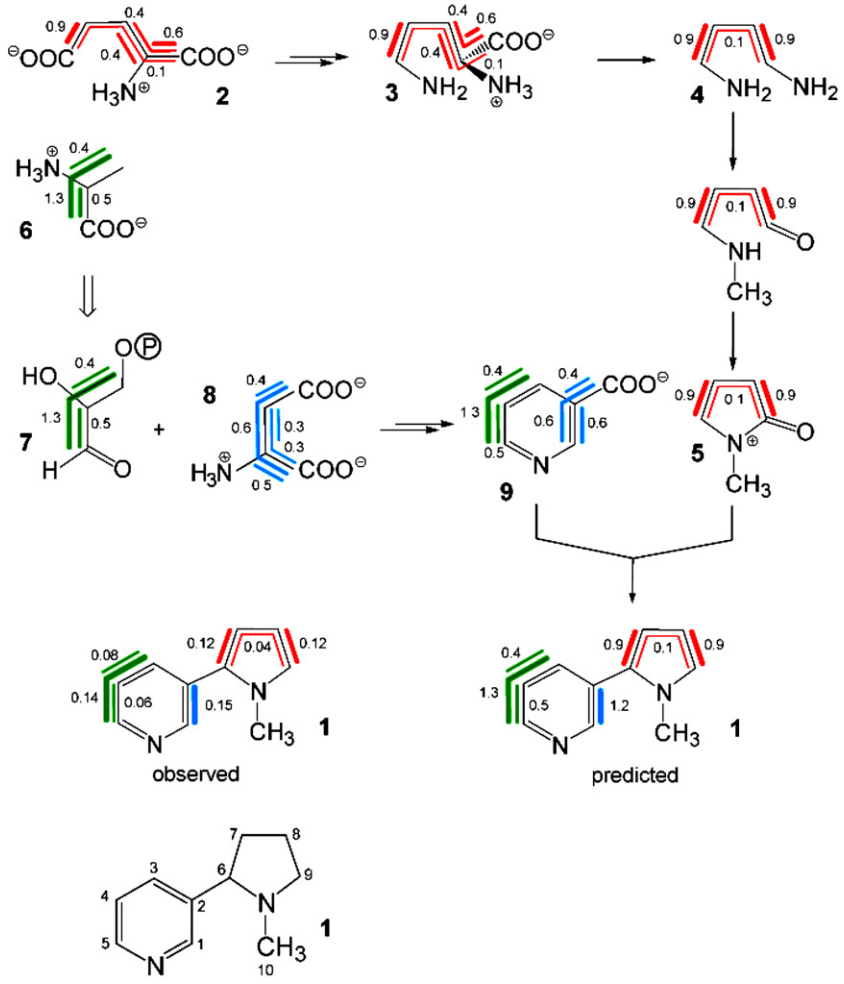

Fig. 10. Isotopologue profiling of nicotine biosynthesis in *N. tabacum* supplied with $^{13}CO_2$. The isotopologue patterns of alanine, aspartate and glutamate are determined by metabolic simulation on the basis of the X-group abundances of glucose and the amino acids (for details, see text). Isotopologues with single blocks of contiguous ^{13}C atoms at molar concentrations of > 0.1 mol% (cf. Tables 6 and 8) are displayed. The labeling pattern of nicotine is inferred from the isotopologue set observed by NMR spectroscopy. On the basis of the labeling patterns in the amino acids, the isotopologue pattern of nicotine is also predicted following known routes of nicotine biosynthesis in *Nicotiana* (for details, see text). Multiple ^{13}C-labeled isotopologues are indicated by bars connecting ^{13}C-atoms within the same molecule. The numbers indicate the abundances of the corresponding isotopologues in mol%. The widths of the bars reflect the relative abundances of the isotopologues. The widths of the bars in nicotine (inferred from NMR spectroscopy) were increased by an approximate value of 10.

Table 10
Stochastic vs. observed isotopologue abundances (mol%) in nicotine from the experiment with $^{13}CO_2$

Isotopologue	Stochastic abundances[a] (mol%)	Observed abundances (mol%)
[1,2-$^{13}C_2$]	0.015	0.15
[3,4-$^{13}C_2$]	0.015	0.08
[3,4,5-$^{13}C_3$]	0.0002	0.14
[4,5-$^{13}C_2$]	0.015	0.06
[6,7-$^{13}C_2$]	0.015	0.12
[6,7,8,9-$^{13}C_4$]	0.000002	0.04[b]
[8,9-$^{13}C_2$]	0.015	0.12
[2,6-$^{13}C_2$]	0.015	0.02[c]

[a] On the basis of the averaged ^{13}C abundance (1.27%).

[b] Derived from the pseudo triplet pattern of ^{13}C-7 and ^{13}C-8 signals at similar intensities both showing simultaneous coupling with the respective carbon neighbours (cf. Table 9).

[c] The observed abundance of [2,6-$^{13}C_2$]nicotine is close to the stochastic abundance and is therefore not displayed in Fig. 10.

in the appropriate pools by matrix multiplication according to $\mathbf{X} = \mathbf{D} \cdot \mathbf{I}$. **X** and **I** are the vectors of X-group and isotopologue distribution, respectively. **D** is the definition matrix of all X-groups (rows), containing only 1 and 0 for isotopologues (columns) included or not included in the respective X-group. A set of sequences is initialised randomly and evolved by a genetic algorithm (GAlib) (Wall, 1996) which uses the rms deviation between the simulated and measured X-groups as a fitness function. The resulting sequences from eight optimised populations were analysed for their relative usage of different pathways.

Acknowledgements

This work was supported by a grant from the Hans Fischer Gesellschaft. We thank Profs. Hartmut Oschkinat

and Helmut Simon for support and discussions and Fritz Wendling for expert technical assistance.

Appendix A. Supplementary data

Supplementary data associated with this article can be found, in the online version, at doi:10.1016/j.phytochem.2007.03.034.

References

Bacher, A., Rieder, C., Eichinger, D., Fuchs, G., Arigoni, D., Eisenreich, W., 1999. Elucidation of biosynthetic pathways and metabolic flux patterns via retrobiosynthetic NMR analysis. FEMS Microbiol. Rev. 22, 567–598.

Breitmaier, E., Haas, G., Völter, W., 1979. Atlas of Carbon-13 NMR Data. Heyden&Son, Philadelphia Rheine, London.

Bush, L., Hempfling, W.P., Burton, H., 1999. Biosynthesis of nicotine and related compounds. In: Gorrod, J. (Ed.), Analytical Determination of Nicotine and Related Compounds and Their Metabolites. Elsevier, Amsterdam, pp. 13–44.

Dauner, M., Sauer, U., 2000. GC–MS analysis of amino acids rapidly provides rich information for isotopomer balancing. Biotechnol. Progr. 16, 642–649.

Dawson, R.F., 1941. The localization of the nicotine synthetic mechanism in the tobacco plant. Science 94, 396–397.

Dewey, L.J., Byerrum, R.U., Ball, C.D., 1955. The biosynthesis of the pyrrolidine ring of nicotine. Biochim. Biophys. Acta 18, 141–142.

Eisenreich, W., Bacher, A., 2000. Elucidation of biosynthetic pathways by retrodictive/predictive comparison of isotopomer patterns determined by NMR spectroscopy. In: Setlow, J.K. (Ed.), . In: Genetic Engineering, Principles and Methods, vol. 22. Kluwer Academic/Plenum Publishers, New York, pp. 121–153.

Eisenreich, W., Bacher, A., Arigoni, D., Rohdich, F., 2004a. Biosynthesis of isoprenoids via the non-mevalonate pathway. Cell. Mol. Life Sci. 61, 1401–1426.

Eisenreich, W., Ettenhuber, C., Laupitz, R., Theus, C., Bacher, A., 2004b. Isotopomer perturbation techniques for metabolic networks, metabolic recycling of nutritional glucose in *Drosophila melanogaster*. Proc. Natl. Acad. Sci. U.S.A. 101, 6764–6769.

Eisenreich, W., Kupfer, E., Weber, W., Bacher, A., 1997. Tracer studies with crude [U-^{13}C]lipid mixtures. Biosynthesis of the lipase inhibitor lipstatin. J. Biol. Chem. 272, 867–874.

Eisenreich, W., Schwarzkopf, B., Bacher, A., 1991. Biosynthesis of nucleotides, flavins, and deazaflavins in *Methanobacterium thermoautotrophicum*. J. Biol. Chem. 266, 9622–9631.

Eisenreich, W., Slaghuis, J., Laupitz, R., Bussemer, J., Stritzker, J., Schwarz, C., Schwarz, R., Dandekar, T., Goebel, W., Bacher, A., 2006. ^{13}C isotopologue perturbation studies of *Listeria monocytogenes* carbon metabolism and its modulation by the virulence regulator PrfA. Proc. Natl. Acad. Sci. U.S.A. 103, 2040–2045.

Eisenreich, W., Strauß, G., Werz, U., Bacher, A., Fuchs, G., 1993. Retrobiosynthetic analysis of carbon fixation in the phototrophic eubacterium *Chloroflexus aurantiacus*. Eur. J. Biochem. 215, 619–632.

Ettenhuber, C., Radykewicz, T., Kofer, W., Koop, H.U., Bacher, A., Eisenreich, W., 2005. Metabolic flux analysis in complex isotopomer space. Recycling of glucose in tobacco plants. Phytochemistry 66, 323–335.

Glawischnig, E., Gierl, A., Tomas, A., Bacher, A., Eisenreich, W., 2002. Starch biosynthesis and intermediary metabolism in maize kernels. Quantitative analysis of metabolite flux by nuclear magnetic resonance. Plant Physiol. 130, 1717–1727.

Hutchinson, C.R., Hsia, M.T., Stephen, C.R.A., 1976. Biosynthetic studies with carbon-13 dioxide of secondary plant metabolites. *Nicotiana* alkaloids. 1. Initial experiments. J. Am. Chem. Soc. 98, 6006–6011.

Katoh, A., Hashimoto, T., 2004. Molecular biology of pyridine nucleotide and nicotine biosynthesis. Frontiers in Bioscience 9, 1577–1586.

Katoh, A., Ohki, H., Inai, K., Hashimoto, T., 2005. Molecular regulation of nicotine biosynthesis. Plant Biotechnol. 22, 389–392.

Lee, W.N., Byerley, L.O., Bergner, E.A., Edmond, J., 1991. Mass isotopomer analysis: theoretical and practical considerations. Biol. Mass Spectrom. 20, 451–458.

Leete, E., 1967. Biosynthesis of the *Nicotiana* alkaloids. XI. Investigation of tautomerism in *N*-methyl-Δ1-pyrrolinium chloride and its incorporation into nicotine. J. Am. Chem. Soc. 89, 7081–7084.

Leete, E., 1958. Biogenesis of nicotine. V. New precursors of the pyrrolidine ring. J. Am. Chem. Soc. 80, 2162–2164.

Leete, E., 1976. A new systematic degradation of nicotine to determine activity at C-2′ and C-5′. The pattern of labeling in nicotine and nornicotine formed from [2-^{14}C]-ornithine in *Nicotiana glutinosa*, and in nicotine obtained from *N. tabacum* exposed to [^{14}C,^{13}C]-carbon dioxide. J. Org. Chem. 41, 3438–3441.

Leete, E., 1992. The biosynthesis of nicotine and related alkaloids in intact plants, isolated plant parts, tissue cultures, and cell-free systems. Environmental Science Research 44, 121–139 (Secondary-Metabolite Biosynthesis and Metabolism).

Leete, E., McDonell, J., 1981. The incorporation of [1-^{13}C, ^{14}C, methylamino-^{15}N]-*N*-methylputrescine into nicotine and scopolamine established by means of carbon-13 nuclear magnetic resonance. J. Am. Chem. Soc. 103, 658–662.

Liebman, A.A., Mundy, B.P., Rapoport, H., 1967. The biosynthesis of nicotine in *Nicotiana glutinosa* from carbon-14 dioxide. Labeling pattern in the pyrrolidine rings. J. Am. Chem. Soc. 89, 664–672.

Mizusaki, S., Tanabe, Y., Noguchi, M., Tamaki, E., 1973. Phytochemical studies on tobacco alkaloids. XVI. Changes in the activities of ornithine decarboxylase, putrescine *N*-methyltransferase, and *N*-methylputrescine oxidase in tobacco roots in relation to nicotine biosynthesis. Plant Cell. Physiol. 14, 103–110.

Nakane, M., Hutchinson, C.R., 1978. Biosynthetic studies of secondary plant metabolites with carbon-13 dioxide. Nicotiana alkaloids. 2. New synthesis of nornicotine and nicotine. Quantitative carbon-13 NMR spectroscopic analysis of [2′,3′,N-CH_3-$^{13}C_3$]nicotine. J. Org. Chem. 43, 3922–3931.

Rohmer, M., 2003. Mevalonate-independent methylerythritol phosphate pathway for isoprenoid biosynthesis. Elucidation and distribution. Pure Appl. Chem. 75, 375–387.

Rueppel, M.L., Mundy, B.P., Rapoport, H., 1974. Biosynthesis of the pyrrolidine ring of nicotine in *Nicotiana glutinosa*. Phytochemistry 13, 141–151.

Sauer, U., 2005. Metabolic flux analysis: a key methodology for systems biology of metabolism. Topics in Current Genetics 13, 191–214.

Schaefer, J., Kier, L.D., Stejskal, E.O., 1980. Characterization of photorespiration in intact leaves using carbon-13 carbon dioxide labeling. Plant Physiol. 65, 254–259.

Schaefer, J., Stejskal, E.O., Beard, C.F., 1975. Carbon-13 nuclear magnetic resonance analysis of metabolism in soybeans labeled by $^{13}CO_2$. Plant Physiol. 55, 1048–1053.

Szyperski, T., 1995. Biosynthetically directed fractional ^{13}C-labeling of proteinogenic amino acids. An efficient analytical tool to investigate intermediary metabolism. Eur. J. Biochem. 232, 433–448.

Van Winden, W., Verheijen, P., Heijnen, S., 2001. Possible pitfalls of flux calculations based on ^{13}C-labeling. Metab. Eng. 3, 151–162.

Wall, M., 1996. GAlib: A C++ Library of Genetic Algorithm Components. Massachusetts Institute of Technology, http://lancet.mit.edu/ga/.